Published in final edited form as:
Comput Chem Eng. 2014 December 4; 71: 715–727. doi:10.1016/j.compchemeng.2014.07.018.

Quantitative Analysis of Robustness of Dynamic Response and Signal Transfer in Insulin mediated PI3K/AKT Pathway

Shibin Mathew[¶,Γ] and **Ipsita Banerjee**[¶,#,§]

[¶]Department of Chemical and Petroleum Engineering, University of Pittsburgh, PA 15261, USA

[#]Department of Bioengineering, University of Pittsburgh, PA 15219, USA

[§]McGowan Institute for Regenerative Medicine, University of Pittsburgh, Pittsburgh, PA 15219, USA

Abstract

Robustness is a critical feature of signaling pathways ensuring signal propagation with high fidelity in the event of perturbations. Here we present a detailed quantitative analysis of robustness in insulin mediated PI3K/AKT pathway, a critical signaling pathway maintaining self-renewal in human embryonic stem cells. Using global sensitivity analysis, we identified robustness promoting mechanisms that ensure (1) maintenance of a first order or overshoot dynamics of self-renewal molecule, p-AKT and (2) robust transfer of signals from oscillatory insulin stimulus to p-AKT in the presence of noise. Our results indicate that negative feedback controls the robustness to most perturbations. Faithful transfer of signal from the stimulating ligand to p-AKT occurs even in the presence of noise, albeit with signal attenuation and high frequency cut-off. Negative feedback contributes to signal attenuation, while positive regulators upstream of PIP_3 contribute to signal amplification. These results establish precise mechanisms to modulate self-renewal molecules like p-AKT.

Keywords

Robust dynamics; Signal transfer efficiency; PI3K/AKT pathway; Self-renewal; Global sensitivity analysis

[Γ]**To whom correspondence should be addressed (during review)**: Tel: 412-642-2071, Fax: 412-624-9639, shm82@pitt.edu.

CONFLICT OF INTEREST

The authors declare that they have no conflict of interest.

1. INTRODUCTION

1.1 Robustness of signaling response

By definition, “A signaling response is robust if it is invariant in the presence of a set of perturbations” (Alderson & Doyle, 2010; Kitano, 2007; Whitacre, 2012). Biological pathways have very similar topology and constraint space as most engineering systems (Chen et al., 2010; Csete & Doyle, 2002; Kiel et al., 2010; Kitano, 2007, 2010; Winterbach et al., 2013); for example chemical process systems (Ogunnaike & Ray, 1994; Seborg et al., 2010). Various experimental and theoretical studies have shown that robustness is a consequence of the evolved topology of signaling pathways; for example presence of signaling hubs and regulatory structures in the pathways (Kitano, 2004; Masel & Siegal, 2009). Signaling hubs decide how signals are channelled from upstream molecules to the downstream molecules and ensure a robust transfer process. Regulatory structures like feedback and feedforward loops promote robustness by regulating the dynamics of information transfer and ensuring efficient control of the signaling process (Behar et al., 2013). These regulatory mechanisms also ensure robust transfer of signals in the presence of noise (Wang et al., 2010). Hence, biological pathways and systems have evolved to elicit robustness like engineering systems which are designed to function robustly (Fisher & Henzinger, 2007).

1.2 Evaluating robustness for systems with uncertainty

1.2.1 Necessity of robustness analysis in hESC self-renewal—hESCs are a promising platform for regenerative medicine applications due to their capacity to self-renew and differentiate into a variety of clinically relevant cell types (Murry & Keller, 2008; Nelson et al., 2009). This cell-fate choice of hESCs is most commonly modulated by application of external chemical cues that activate a number of intracellular signal transduction pathways (W. Li et al., 2013; Mathew et al., 2012). These pathways relay extracellular information to the internal processes in the cell (eg. gene transcription in nucleus) to orchestrate a particular response.

An area of intense research is to develop a defined platform for the maintenance of self-renewal of hESCs. Initial methods to maintain self-renewal involved feeder layers like mouse fibroblasts that secreted essential factors (Thomson et al., 1998). Further research identified the chemistry of the secreted factors and led to the development of synthetic substrates and growth media that mimic these feeder layers (Kleinman & Martin, 2005; Ludwig & Thomson, 2007). Current efforts are directed towards the identification of defined chemical cocktails that can target specific nodes of the signaling pathways and increase the self-renewal capacity of these cells (Desbordes et al., 2008). Such a shift will benefit the replacement of many factors from the current culture conditions that have xenogenic origin.

Systems like hESCs have high degree of cell-to-cell variability in the expression levels of many signaling proteins (Cahan & Daley, 2013). This variability can significantly influence the properties of signal transfer. Nevertheless, experiments have shown that most cellular systems have evolved to elicit robust responses even in the presence of external and internal perturbations (Csete & Doyle, 2002; Kitano, 2004; Stelling et al., 2004). This is also true for

hESCs, where many experimental protocols exist to robustly maintain self-renewal or direct differentiation to various lineages (Agarwal et al., 2008; D'Amour et al., 2006; Yao et al., 2006). This robustness of cellular response is a consequence of "robust transfer of signals" through the signaling pathway (Bluthgen & Legewie, 2013). Hence, the objective of this paper is to evaluate the robustness promoting mechanisms in the self-renewal PI3K/AKT pathway in hESCs.

1.2.2 Metrics to quantify robustness—Quantitative treatment of network level robustness for biological systems was first advocated by Kitano in a set of pioneering papers (Kitano, 2007, 2010). In these papers, Kitano outlined the use of 'evaluation functions' to describe deviation of response of an important molecule of the network from the nominal case under a particular set of perturbations. An example of the response could be maintenance of levels of signaling molecules at a nominal value. The evaluation function is defined for every parameter combination in a particular set and the perturbations are weighed by the probability of their occurrence. Averaging the weighted evaluation function over the entire parameter space of the perturbation set gives a measure of the total robustness of the network to this set. Several modifications to these robustness measures exist based on the mathematical tool used for the application at hand. These include; 'violation and satisfaction degree' based on linear temporal logic formulae (Rizk et al., 2009), single and multi-parameter 'degree of robustness (DOR)' score based on bifurcation points (Blüthgen & Herzel, 2003; Ma & Iglesias, 2002), 'viable volume' based on sampling strategies like Monte Carlo (MC) sampling (Eissing et al., 2005) and hybrid global and local sampling (Zamora-Sillero et al., 2011), 'singular value of perturbations' based on structured singular value analysis (Luni & Doyle III, 2011).

1.3 Robustness evaluation of PI3K/AKT pathway in self-renewal state

1.3.1 PI3K/AKT pathway interactions—Insulin and insulin-like growth factor 1 (IGF-1) is a prime component of many cell culture systems and results in the activation of many important pathways regulating cell survival, metabolism, proliferation etc. (Bendall et al., 2007; Kiselyov et al., 2009; Sedaghat et al., 2002). A common upstream pathway associated with these effects is the PI3K/AKT pathway (Sedaghat et al., 2002). In cellular systems like hESCs, the pathway has additional roles, namely promotion of self-renewal and inhibition of differentiation signals (Dalton, 2013). The pathway has two major modules (Figure 1A–B). Module 1 includes receptor level processes, namely receptor activation by the ligand, internalization into endosomes, recycling back to the surface and their production and degradation. Module 2 includes tyrosine phosphorylation of receptor substrate (IRS1), complexation of IRS1 with PI3Kinase, production of phosphoinositol lipids followed by activation of AKT. The pathway also has several regulatory loops; these include negative feedback via downstream kinases like PKC-ζ, negative regulators like PP2A, PTEN, SHIP, PTP and double negative feedback via p-AKT on PTP.

In this pathway, AKT acts as a central hub of the pathway and the dynamics of AKT is decoded by downstream molecules in different ways to regulate important cellular processes like protein synthesis via mTORC1/p70S6K, glycogenesis via GSK3β, gluconeogenesis via G6Pase (Behar & Hoffmann, 2010; Kubota et al., 2012). The levels of p-AKT correlate well

with the self-renewal or differentiation propensity of hESCs, high levels promoting self-renewal and low levels promoting differentiation (Singh et al., 2012). The mathematical model of this pathway under nominal parameters was previously studied exclusively to changes in insulin stimulation in different cell systems like adipocytes (Giri et al., 2004; Sedaghat et al., 2002) and was recently validated by us for self-renewing hESCs under steady state (Mathew et al., 2014).

1.3.2 Signal transfer properties of the pathway—Due to the critical role of the PI3K/AKT pathway, it is essential to understand how levels of molecules like p-AKT are regulated and identify key perturbations which can cause variability in the p-AKT levels. We have recently demonstrated an overshoot behavior in the post receptor molecules in the hESC system under self-renewal which is under the control of negative feedback (Mathew et al., 2014). The overshoot behavior ensures a speedy response with a fast settling down to intermediate levels. Loss of the negative regulatory processes can lead to hyperactivation of the pathway, as is commonly observed in pathological states like cancer (Andersen et al., 2004; Scott et al., 2010; Zhang, 2005). Inhibition of negative feedback changes the dynamic response of the pathway and p-AKT levels now show a first order increase instead of the overshoot behavior. Identification of factors that can lead to maintenance of a robust (overshoot or first order) response and removal from a robust region will help in the discovery of efficient targets to modulate the response according to the context. A recent study looked at the quantitative features of robust signal transfer in this pathway for heregulin mediated activation (Tian & Wu, 2013). In this paper, we present a thorough quantitative analysis of robustness of the pathway for insulin stimulation considering the entire pathway and using the parameter ranges that are known to give rise to the two major dynamic responses: the overshoot response represents the self-renewal state of hESCs and the first order response represents a possible perturbed case.

To analyze the robustness of response from the PI3K/AKT pathway under insulin stimulation, we considered two type of perturbations. Firstly, we considered the influence of perturbations in the pathway parameters in maintaining a given dynamic response. Secondly, we considered the propagation of signal from insulin ligand to the internal molecules given a noisy signal. We tested various oscillatory scenarios of insulin stimulus to study the noise filtering capabilities of the PI3K/AKT pathway. Our results suggest that negative feedback in the pathway plays an important role in maintaining a robust nominal response. In the absence of which, the pathway gains sensitivity to many perturbations associated with the cascade reactions. Further, the pathway has the capability to attenuate oscillations and paradoxically, the degree of attenuation increases with the increase in freqency of the oscillations. In combination with parameter pertubations, our results present various mechanisms to ensure a robust signal transfer in the pathway.

2. METHODS

2.1 Modeling formalism and computations

The dynamics of interactions in Module 1 and 2 of the pathway is described by ordinary differential equations (ODEs). The current mathematical model assumes a continuum of

states under a deterministic reaction scheme with each reaction modeled primarily using mass-action kinetics and negative feedback modeled using a Hill type kinetics. Original mathematical model of this pathway is based on Sedaghat *et al.* model for adipocytes (Sedaghat et al., 2002). In our previous work, we extended the basic model and modified the Sedaghat model for application to self-renewing population of hESCs (Mathew et al., 2014). The resulting model has 27 reactions, 20 output species and 31 rate parameters. From the rate parameters, 25 were selected as free inputs for our analysis while the remaining parameters were specified as functions of these selected inputs (Mathew et al., 2014). Other input parameters included the concentrations of the molecules PTP, PTEN and SHIP and the input insulin concentration (see Table 1). The initial conditions are kept same as (Sedaghat et al., 2002). All computational codes were written in FORTRAN R90 and the ODEs were integrated using DLSODE solver (Hindmarsh, 1983). The computations were carried out on INTEL® Core™ 2 Quad CPU (Q8400 @ 2.66GHz).

2.2 Robustness quantification under parameter uncertainty

The robustness measure adapted here is inspired from the work of Kitano where a evaluation function was used to denote the deviation of the system response from the expected response (Kitano, 2004, 2007). In this work, the evaluation function is used to quantify the deviation from a behavior selected to be robust. To simulate perturbations, each rate parameter, k_i, is chosen by the relation,

$$k_i^{(s)} = k_i^{nom} 10^{x^{(s)}} \quad (1)$$

Here, $x^{(s)}$ is a random number sampled from a uniform distribution within the range, [−σ, σ]. k_i^{nom} is the nominal value of the rate parameter, *i*, defined in Table 1. The superscript, *s*, stands for the sample number. Let *n* be the total number of free parameters chosen for the analysis. For a given parameter set vector, $\bar{k}^{(s)} = (k_1^{(s)}, k_2^{(s)}, \ldots, k_n^{(s)})$, and the nominal parameter set, $\bar{k}^{nom} = (k_1^{nom}, k_2^{nom}, \ldots, k_n^{nom})$, the evaluation function, R_{dyn} ($k^{(\bar{s})}$), is defined by the relation,

$$R_{dyn}(\bar{k}^{(s)}) = \frac{1}{1 + \frac{1}{t_{steps}} \sum_{j=1}^{t_{steps}} \left[\frac{Y_j(\bar{k}^{(s)}) - Y_j(\bar{k}^{nom})}{Y_j(\bar{k}^{nom})} \right]^2} \quad (2)$$

The evaluation function is defined for every sample *s* and output *Y* (for example, p-AKT). The term in the denominator measures the square of the deviation of Y_j at a given time step, *j*, from the nominal value at the same time step. This term is then averaged over all time steps, $j = 1, \ldots, t_{steps}$. For current analysis, a step size of 0.1 min is used and the dynamics is simulated till 20 min (Hence, $t_{steps} = 200$) where most of the time profiles reach steady state. Further reduction in the step size did not increase the accuracy of the results. The evaluation function takes values in the range [0,1]. For a significantly large deviation from the nominal dynamic profile, the evaluation function tends to zero, while for negligible deviation, its value tends to one. Several MC samples were generated in the high dimensional parameter space and the entire collection of these samples constitutes a perturbation set, $K = \{k^{(\bar{1})}, k^{(\bar{2})}, k^{(\bar{3})}, \ldots, k^{(\bar{s})}, \ldots, k^{(\bar{N})}\}$, where *N* denotes the total number of samples.

The overall robustness score, $R_{overall}(K)$, of the pathway is defined for a perturbation set, K, by the relation,

$$R_{overall}(K)=\int_{k_1}\int_{k_2}\dots\int_{k_n} R_{dyn}(\bar{k})dk_1dk_2\dots.dk_n \quad (3a)$$

In the current work, the multi-dimensional integral in the Equation (3a) is approximated by MC integration. For each parameter selected independently, Equation (3a) can be approximated as:

$$R_{overall}(K) \approx \frac{\prod_{i=1}^{n}[\Delta k]_i}{N}\sum_{s=1}^{N} R_{dyn}(\bar{k}^{(s)}) \quad (3b)$$

Here, Δk_i refers to the range of the interval for the parameter i and is equal to $k_i^{nom}\times[10^{\sigma}-10^{-\sigma}]$ based on Equation (1). After division with the volume factor, $\prod_{i=1}^{n}[\Delta k]_i$, the normalized robustness score is given by:

$$\tilde{R}_{overall}(K) \approx \frac{1}{N}\sum_{s=1}^{N} R_{dyn}(\bar{k}^{(s)}) \quad (3c)$$

It is important to note that every perturbation in Equation (3a) is equally likely due to the uniform distribution assumption in Equation (1). Selecting different values of σ varies the extent of perturbation.

2.3 Global sensitivity analysis (GSA)

2.3.1 Variance decomposition—Global sensitivity analysis was performed to evaluate the contributions of different parameters to the changes in the evaluation function, $R_{dyn}(\bar{k}^{(s)})$, in the high dimensional parameter space. We used variance decomposition process that conveniently decomposes the variance in the output (σ^2) into several components contributed by the perturbed parameters $(\sigma_i^2,\sigma_{ij}^2,\dots.)$ (Sobol′, 2001). Here, σ_i^2 denotes the contribution of a single parameter, k_i, σ_{ij}^2 denotes the contribution of pairs of parameters, (k_i, k_j), and so on. For a total of n free parameters, this can be written as:

$$\sigma^2=\sum_{1\le i\le n}\sigma_i^2+\sum_{1\le i<j\le n}\sigma_{ij}^2+\dots.+\sigma_{1,2,3,\dots.,n} \quad (4)$$

To evaluate each term in Equation (4), we use an alternate approach of function decomposition, where the evaluation function itself is decomposed into independent hierarchical component functions corresponding to each term in Equation (4). The function decomposition is defined as,

$$R_{dyn}(\bar{k})=F_0+\sum_{1\le i\le n}F_i(k_i)+\sum_{1\le i<j\le n}F_{ij}(k_i,k_j)+\ldots.+F_{1,2,3,\ldots,n} \quad (5)$$

Each term in Equation (5) is defined as follows:

Mean, $F_0 = E(R_{dyn}(k))$

First order, $F_i(k_i)=E(R_{dyn}(\overline{k_{-i}})|k_i) - F_0$

Second order, $F_{ij}(k_i,k_j)=E(R_{dyn}(\overline{k_{-ij}})|k_i,k_j) - F_0 - F_i(k_i) - F_j(k_j)$

N[th] order,

$$F_{1,2,3,\ldots,n}=R_{dyn}(\bar{k})-F_0-\sum_{1\le i\le n}F_i(k_i)-\sum_{1\le i<i\le n}F_{ij}(k_i,k_j)-\ldots.-upto(n-1)^{th}\ term$$

Each component function contains high dimensional integrals that are evaluated as special instances of the ODE output. For example, $E(R_{dyn}(k))$ is the expected value of the evaluation function in the entire hyperspace, $E(R_{dyn}(\overline{k_{-i}})|k_i)$ is the conditional expectation of the evaluation function at a given k_i. $\overline{k_{-i}}$ stands for the vector of parameters without k_i and $\overline{k_{-ij}}$ stands for vector of parameters without k_i and k_j. Higher order terms can be evaluated likewise. For most physical systems, expansion in Equation (5) converges by the second order term and therefore, second order is sufficient for a good representation of the system (G. Y. Li & Rabitz, 2012; Mathew et al., 2014). Traditional methods like MC integration for evaluation of these component functions would require large number of samples as well as repeated sampling (for different conditional expectations) (Feil et al., 2009). To reduce the computational cost of this process, we employed Random Sampling High Dimensional Model Representation (RS-HDMR) described in detail by (G. Y. Li & Rabitz, 2012). For the results in this manuscript, it was found that the second order indices were sufficient to explain most of the variance of the data. The higher order indices were comparatively less important and hence a second order RS-HDMR will be discussed further.

2.3.2 RS-HDMR Meta-model algorithm—RS-HDMR is a multivariate regression technique that approximates the component functions in Equation (5) as mixtures of orthonormal functions to reduce the computational effort. Based on (G. Y. Li & Rabitz, 2012), these function approximations can be written as follows:

First order, $F_i(x_i) \approx \sum_{1\le p\le u}\alpha^i{}_p\phi^i{}_p(x_i)$

Second order, $F_{ij}(x_i,x_j)=\sum_{1\le q\le v}\sum_{1\le r\le w}\beta^{ij}{}_{qr}\varphi^i{}_q(x_i)\varphi^i{}_r(x_j)$

RS-HDMR requires the input parameters to lie in the range [0,1]. Hence, the free parameters, k_i, in Equation (5) are replaced by another parameter, x_i, in the range [0,1] and these are related by $k_i=[k_i^{nom}10^{-\sigma}+k_i^{nom}(10^{\sigma}-10^{-\sigma})x_i]$. The integers *u*, *v*, *w* are orders of the orthonormal polynomials, ϕ, and are usually taken as ≤ 3 (G. Li et al., 2010). The coefficients $\alpha^i{}_p$ and $\beta^{ij}{}_{qr}$ are determined as described in (G. Y. Li & Rabitz, 2012).

2.3.3 Sobol' indices—Sobol' indices capture the sensitivity of the output to a selected parameter. By definition, first order indices are evaluated as, $S_i=\frac{\sigma_i^2}{\sigma^2}$ and similarly, second order indices are evaluated as $S_{ij}=\frac{\sigma_{ij}^2}{\sigma^2}$ and so on. The total variance, σ^2, is calculated from the data and the individual variances are related to the coefficients of the component function presented in Section 2.3.2 by $\sigma_i^2=\sum_{1\le p\le u}\left(\alpha^i{}_p\right)^2$ and $\sigma_{ij}^2=\sum_{1\le q\le v}\sum_{1\le r\le w}\left(\beta^{ij}{}_{qr}\right)^2$. See (G. Y. Li & Rabitz, 2012) for derivations of these relationships.

3. RESULTS AND DISCUSSION

3.1 PTP acts as a control point for changing dynamic response of PI3K/AKT pathway

We started with a well-defined mechanistic model of the PI3K/AKT pathway (Sedaghat et al., 2002) which was recently extended and validated for the self-renewing hESC system (Mathew et al., 2014). It is known that the maximal activation (or maximal phosphorylation status) of the PI3K/AKT pathway molecules for a given insulin dose is largely modulated by the negative regulators of the pathway, like PTP, PTEN and negative feedback via kinases like PKC-ζ (Alva et al., 2011; Gafni et al., 2013; Kwei et al., 2008; Luni et al.; Mathew et al., 2014; Sedaghat et al., 2002; Yoon et al., 2010). Further, the dynamic response of signal transduction depends on the relative strength of the positive and negative regulators, particularly for long term signaling (Sedaghat et al., 2002). When positive regulators dominate, we see a first order response while when negative regulators dominate, we see an overshoot behavior (Sedaghat et al., 2002). Among the negative regulators, PTP is responsible for negative regulation of both the modules of the pathway, for example dephosphorylation of active insulin receptors (Module 1) and dephosphorylation of important downstream kinases like IRS1 and PI3K (Module 2). Based on this role, it is known that inhibition of PTP leads to abnormal tyrosine phosphorylation of the pathway while, activation of PTP leads to suppression of active molecules of the pathway (Mahadev et al., 2001; Nguyen et al., 2013; Smith & Shanley, 2013). Figure 2A shows the steady state phosphorylation levels of four molecules from different sections of the pathway, namely p-IR (active surface receptors), p-IRS1 (tyrosine, Y), p-IRS1 (serine, S) and p-AKT for different basal PTP levels. For high PTP levels, there is not much dependence of the levels of the four molecules on PTP. For levels less than 0.1, we see rapid changes in the levels of these molecules and there is abundant tyrosine phosphorylation of IR and IRS1 and very low serine phosphorylation of IRS1. Apart from the steady state response, PTP levels also change the temporal response of the pathway. Figure 2B shows the temporal profiles of the key molecule p-AKT for different PTP levels simulated for the first 40 min post stimulation. For PTP = 1, we see the regular overshoot behavior while with decreasing PTP levels, there is a shift to a first order response (PTP < 0.01). The overshoot behavior is the result of negative feedback by downstream kinase, PKC-ζ. This effect is lost under hyperactivation of the pathway at PTP = 0 leading to negligible influence of negative feedback. This is also indicated by substantial reduction in negative feedback molecule, p-IRS1 (S), as PTP tends to 0 (Figure 2A). Thus, the level of PTP can decide the nature of the dynamics of the pathway molecules, first order or overshoot.

Since different dynamics of key signaling molecule of the pathway like AKT can lead to different downstream cellular response (Kubota et al., 2012), it is important to precisely control not only the actual levels but also the dynamics of the pathway. Modulation of PTP levels provides a convenient way to modulate the dynamics and hence we chose presence or absence of PTP as a switch to enforce these divergent dynamics. Maintaining either of these two dynamics would depend upon the influence of other parameters. Therefore, we next investigated how robustly these dynamic responses are reproduced under varying degrees of parameter perturbations.

3.2 Influence of parameter uncertainty on dynamic response for extreme PTP levels

Obtaining a robust response (whether regular or pathological) in the presence of uncertainty will depend on the sensitivity of the kinetic parameters in the respective regimes (Kitano, 2004, 2007). To study how parameter uncertainty influences a nominal state (PTP = 1) and a perturbed state (PTP = 0), we first simulated the temporal profiles of a key downstream molecule p-AKT for different degrees of perturbation in the 28 parameters and a step input of a saturated concentration of insulin (10^{-7} M). The parameters were randomly chosen assuming a uniform distribution using the relation in Equation (1) for different levels of perturbation parameter, σ. The perturbation parameter decides the interval of each parameter from which a random sample is generated. For each σ, 10^5 MC samples were generated. σ levels of 0.01, 0.02, 0.05 and 0.1 correspond to 2, 4, 12 and 25% deviation of the rate parameters from their nominal values.

Figure 2C–D shows the dynamics of p-AKT for PTP = 0 and PTP = 1 respectively. The shaded regions represent the clusters of p-AKT profiles under different degrees of perturbation and the red curve shows the nominal dynamics. We observe that increasing σ from 0.01 to 0.05 causes the p-AKT levels to shift from their nominal values, however the nature of dynamics of the profiles remain the same. For PTP = 0, final p-AKT values range from 10 to 25% and for PTP = 1, the values range from 5 to 12%. Interestingly, we see a faithful reproduction of the time to saturation (when PTP = 0) and time to peak (when PTP = 1) irrespective of the parameter perturbation. It was noticed that increasing σ values further resulted in profiles that deviated from the nominal dynamics for each of the two PTP levels, indicating that it is difficult to maintain the same dynamics for large σ. Figure S1 shows the deviation from nominal behavior at a σ of 0.5 (which corresponds to a total deviation of 200% from the nominal value). This analysis shows that information on the local p-AKT dynamics is preserved for perturbations at least until σ = 0.05, increasing σ leads to samples with divergence in the dynamics. To identify the relative influence of uncertainty in each parameter on the different output profiles, it is necessary to quantify the extent of deviation from the nominal profile.

3.3 Parameter perturbations affecting robustness of p-AKT dynamics

3.3.1 Quantification of overall robustness as a function of σ—The overall robustness score presented in Equation 3 is a measure of the average influence of all the perturbations in a selected parameter space. Using the parameter sets from Figure 2C–D, we calculated the evaluation function, $R_{dyn}(\bar{k})$, for each MC sample for σ ranging from 0.01 to 0.5 using Equation 2. This score represents the degree of deviation in the dynamics of p-

AKT produced by a perturbed parameter set for a given PTP value. A high score close to 1 indicates that the perturbation has not produced a significant deviation. Scores close to 0 indicate that the perturbation has resulted in very large deviations and hence the profiles are no longer in the local region of the nominal curves. For robustness quantification, the p-AKT profiles were simulated till 20 min, when most of the samples had reached levels close to their steady state. One the evaluation function was estimated for each parameter combination, the overall robustness score was calculated as an average evaluation score. We ensured that the estimates had reached convergence for the selected number of MC samples (10^5 samples were required). Figure 3A presents the overall robustness score for increasing σ values. For both PTP levels, the robustness score for σ values from 0.01 to 0.05 remain in the range [0.8,0.99], indicating that these perturbations are robust enough to maintain the p-AKT profiles close to the nominal. Further increase in σ results in a very poor robustness score indicating that these perturbations have resulted in significant deviations from the expected dynamics. For a given σ, the overall robustness score is slightly higher for PTP = 0 than PTP = 1. This is because the nominal p-AKT levels are lower for PTP = 1 than PTP = 0. As the robustness scores are normalized to the nominal p-AKT levels, this leads to a slightly higher robustness score for PTP = 0 than PTP = 1.

3.3.2 Global sensitivity of evaluation function, $R_{dyn}(\bar{k})$, to parameter perturbations—

The results from Section 3.3.1 quantifies the overall deviation of the system, but it does not resolve the effect of individual parameters and processes. To quantify this influence, we chose to perform a parameter sensitivity analysis on the evaluation function. However, it is necessary to identify the combined influence of different parameters due to the non-linearity of the model. Therefore, we performed a global sensitivity analysis (GSA) of the $R_{dyn}(\bar{k})$ score for a σ of 0.05, where the dynamics for a given PTP is conserved. Global sensitivity captures the influence of a chosen parameter under simultaneous variations in the other parameters. Hence it can capture the effect of parameters acting in isolation, along with that in combination with other parameters. We chose a variance-based approach to quantify the contribution of variance in different parameters to the total variance in the perturbed parameter space. The effect of these perturbations are captured in Sobol' indices as discussed in the Section 2.3.3. First order indices capture the influence of a single parameter while second order indices capture the influence of pairs of parameters and so on. To reduce the computational cost of GSA, we chose a RS-HDMR meta-model based approach. The meta-model replaces the ODE while evaluation of the Sobol' indices. We recently demonstrated the accuracy and computational efficiency of RS-HDMR for the same PI3K/AKT pathway model (Mathew et al., 2014) developed for a system of self-renewing hESCs.

A second-order RS-HDMR meta-model was used to evaluate the first order and second order Sobol' indices for $R_{dyn}(\bar{k})$ for PTP = 0 and PTP =1. For both cases, the first order Sobol' indices were negligible and contributed to 1% of the variance. The second order indices were significant and contributed to 75% of the variance. Figure 3B shows a heat-map of the second order Sobol' indices for the two cases. The upper half triangle presents the indices for PTP = 1 and the lower half presents the indices for PTP = 0. We observe that most of the perturbations have very small contributions to the output. Therefore, the

pathway is robust to most perturbations, yet sensitive to some key perturbations. The phosphorylation-de-phosphorylation rate of AKT (k_{11}, k_{-11}) is the most sensitive combination and it is common to both cases. These parameters are also involved in second order interactions with other sets of parameters. The secondary interactions are, however, different for the two cases. For PTP = 1, there is significant contributions from parameters associated with negative feedback via PKC-ζ. These include the parameter affecting the levels of p-PKC-ζ (k_{12}, k_{-12}) and parameter influencing the half-maximal rate of serine phosphorylation of IRS1 (K_d). Thus, the modulation of the negative feedback parameters can affect the robustness of the response when PTP = 1. Changes in the other parameters will not have any consequence on the robustness of the response in this regime and selected degree of perturbation. For PTP = 0, the secondary contributions are from parameters affecting the activation and deactivation of upstream molecules PI3K and PIP_3 (namely, k_8, k_{-8}, k_{9stim}, k_{-9}). These additional parameters also interact with the levels of PTEN. Thus, parameters affecting the upstream molecules of AKT primarily influence the dynamics of AKT in this regime with negligible contribution from the negative feedback parameters.

Parameter combinations in Figure 3B indicate the combined action of two parameters on the evaluation function. For a given pair, when both the parameters are kept at the nominal levels (center of the perturbation interval), the dynamics is nominal. When one of them is perturbed away from the nominal values, the evaluation function worsens since the equilibrium relation between them is perturbed. This is illustrated in Figure 3C–D, where R_{dyn} (k) is plotted against the right half of the interval of the most sensitive parameter, k_{-11} for each of the two PTP levels and a σ of 0.05. The black curve shows that as k_{-11} increases, R_{dyn} (k) decreases due to the increased de-phosphorylation of AKT. This can be rescued by the simultaneous increase in phosphorylation rate k_{11}. For example, the blue curve in Figure 3C shows the influence of k_{-11} when the parameter k_{11} is kept at the higher end of the perturbation interval. Here, R_{dyn} (k) increases above the black curve when k_{-11} is above 0.68. PTEN is another parameter that is found sensitive in combination with k_{-11}. Decrease in PTEN can rescue the worsening of R_{dyn} (k_i) produced by increasing k_{-11} as shown by green curve in Figure 3C. When R_{dyn} (k_i) approaches 1, the modulated parameter restores the perturbation induced by change in k_{-11}. Here, reduction in PTEN increases the levels of upstream activator of AKT (PIP_3) and compensates for the reduction in AKT by increased de-phosphorylation. Simultaneous perturbation of (PTEN and k_{11}) suppresses the phosphorylation more than the required amount and it is difficult to increase the R_{dyn} (k_i) levels (red curves in Figure 3C). Similar observations can be made with decrease in phosphorylation rate of PKC-ζ (k_{12}) or increase in the phosphorylation rate (k_{11}), when PTP = 1 (see green and blue curves respectively, in Figure 3D with their combined action presented by red curve in Figure 3D). For negative feedback, we see a peak in R_{dyn} (k_i) between k_{-11} of 0.7 and 0.8 after which it decreases again. These relationships establish the compensatory nature of different perturbations as is commonly observed in biological models and can be uncovered easily using meta-model based global sensitivity tools.

To summarize this section, negative feedback is the most dominant process in the local region of PTP = 1 and it promotes robustness of the pathway to perturbations in the other parameters. In the absence of negative feedback, the pathway becomes highly sensitive to

perturbations involving the upstream activation and deactivation mechanisms. Our analysis also shows that the receptor level processes are decoupled from the post-receptor processes of the PI3K/AKT pathway for concentration of insulin relevant to *in vitro* systems. This decoupling between the two modules was also seen in PC12 cells under activation of the epidermal growth factor signaling (Fujita et al., 2010).

Until now, the emphasis was on fidelity of the dynamic response under variability associated with the rate parameters and the negative regulators. Here, we selected a constant input stimulus and a predefined output response and then studied the contributions of different parameters on a specific output. While this captures how internal variability affects transduction of a fixed input, it does not explain how fluctuations in the input signal propagate downstream. To study this, we need to modulate the concentrations of insulin and evaluate the corresponding changes in the downstream molecules. Robustness against input signal variability has two contrasting objectives: elimination of noisy inputs but preservation of fidelity (Toyoshima et al., 2012; Wang et al., 2010). In the following sections we evaluated the signal transfer efficiency of the pathway under combinatorial variations in the pathway parameters and oscillatory input insulin scenarios.

3.4 Robustness of signal transfer in the PI3K/AKT pathway

Modulation of input signal dynamics are commonly represented by step, ramp or pulse inputs. Along with the nature, there can be variations in magnitude and duration of the signal. Cyclic inputs offer a convenient method to explore various combinations of magnitude (amplitude) and duration (period or (frequency)$^{-1}$). Biologically, such oscillations can arise due to various reasons: they may be imposed due to cyclic changes in physiological state of the organism *in vivo*, or they may be a direct consequence of periodic changes in external media which is more relevant for *in vitro* systems. In addition to the dynamics of the input signal, there may be noise in the input imposed by ambient fluctuations. Hence, for the analysis of signal transfer, we chose two scenarios: (1) oscillatory signals of varying amplitude and frequency and (2) oscillatory signals with superimposed noise. The input oscillations are introduced into the system after it reached steady state corresponding to an input insulin level of 10^{-9} M. For the following analysis, total time of 300 min is allowed before oscillations are introduced.

3.4.1 Robust signal transfer without noise

3.4.1.1 Single Square waveform input: We first started with a single square waveform in the insulin levels as defined in Figure 4. The total duration of the single cycle was varied between 200 min to 20 min and the resulting perturbation in the steady state levels of four major outputs of the pathway, p-IR, p-IRS1 (Y), p-IRS1 (S) and p-AKT were recorded. As seen from Figure 4, for a total duration of 200 minutes, all the outputs follow the cycle in insulin levels very closely. At the beginning of the cycle (red curve), when the molecules sense a step increase in insulin levels from 10^{-9} to 10^{-8} M, there is rapid increase in the active levels of the molecules to their peak values. Then, p-AKT and p-IRS1 (Y) show a rapid decrease to steady state levels and p-IR shows a gradual decrease due to the internalization and deactivation of the receptors. p-IRS1 (S), however, stays at the peak level. At 400 min, when the insulin levels decrease to a low level of 10^{-10} M, all the

molecules respond by decreasing their activity, but they reach the new steady state levels gradually (in 25 min as compared to 5 min for the activation part). It takes close to 50 minutes to reach the steady state. Interestingly, the pathway responds very quickly to changes in the insulin levels even during deactivation portion of the cycle, but the time to reach the corresponding steady state can be quite different for activation and deactivation cycles. Due to this asymmetry, the molecules respond differently when the cycle period is decreased. As expected, the amplitude of the downward part of the cycle is highly reduced when the cycle period is decreased below 50 min. When the cycle duration is 20 min, none of the outputs remain responsive to changes in insulin levels. This demonstrates that the PI3K/AKT pathway has the ability to cut-off cycles of a certain frequency. Any square input waveform of insulin with a period less than 20 min or frequency greater than 0.05 min^{-1} will not be transmitted down the pathway. In general, the pathway recognizes oscillations of sufficient amplitude and period as signal and transmits them downstream and shuts down the transmission of very low period signals. This filtering effect is observed in other systems as well and is a complex function of the amplitude of the oscillations and the strengths of different processes contributing to signal transmission (Gomez-Uribe et al., 2007; Wang et al., 2010).

3.4.1.2 Sinusoidal waveform: For a more general analysis, we subjected the insulin levels to a sinusoidal change given by $Ins(t) = Ins(0)(1+ a \sin(\omega (t - 300)))$. This gives us a convenient way to study modulations in the amplitude (a) and frequency (ω) of oscillations. For our analysis, the basal insulin levels ($Ins(0)$) are kept constant at 10^{-9} M before 300 minutes after which the oscillations are started. Figure 5 shows the resulting oscillations in the input and the four outputs respectively. The oscillations were introduced at amplitude of 0.9 and frequency of 0.01 min^{-1}. For the plot, the output is measured as the ratio of the actual level of the molecule to the mean level under oscillations. Transfer efficiency of a signal is captured by the amplitude, frequency and phase of the output oscillations relative to the input oscillations. From Figure 5, it is seen that the oscillations are faithfully transmitted down the pathway with the same frequency and phase. For p-IR, p-IRS1 (Y) and p-AKT, there is attenuation of the output amplitude to 0.5 compared to the input amplitude of 0.9. For p-IRS1 (S), the output amplitude is relatively higher at 0.8 indicating higher signal transfer efficiency. Thus, under nominal conditions, the signal is transmitted down the pathway with some attenuation.

3.4.1.3 Parametric dependence of signal transfer efficiency: Modulation of signal parameters and pathway parameters can control the degree of attenuation of signal transfer down the pathway (Wang et al., 2010). In this section, we investigated the influence of pathway parameters on the signal transfer efficiency for oscillatory inputs. Figure 6A shows the influence of input frequency and amplitude of insulin on the output amplitude of p-AKT and nominal parameter values. Three different input amplitudes were chosen, namely 0.9, 0.7 and 0.5. Although only the features of p-AKT output are presented here, same conclusions can be drawn for the other molecules. As seen from Figure 6A, we see a flat response in p-AKT output amplitude for low frequencies. In this region, the output amplitude is “attenuated” as compared to the input amplitude. For example, the ratio of output to input amplitude is 0.6, 0.43 and 0.4 for input amplitudes of 0.9, 0.7 and 0.5

respectively. The decrease in this ratio with decrease in amplitude shows that there is an increase in signal attenuation at lower input amplitudes. Hence, increasing the amplitude of the oscillations will favor its transduction down the pathway. For $\omega > 0.1$, there is linear decrease in the output amplitude indicating a "filtering" of input oscillations. Further, for very high ω ($\log_{10}(\omega) > 0.5$), the amplitude of the output is negligible and independent of the amplitude, thus indicating "cutoff" of high frequency oscillations. To analyze the importance of pathway parameters on these observations, we kept the input amplitude constant at a high value of 0.9 for further analysis. This amplitude ensures the input signal varies in a large range without leading to values that are negative or close to zero. The input frequency was varied in the range [0.01, 10] with simultaneous variation in the parameters of the model (for $\sigma = 0.5$). A higher σ was chosen to incorporate all possible dynamic regimes. Figure 6B shows the output amplitude of p-AKT as a function of input ω for 10^5 MC samples. As seen from the figure, for very low ω, there is a high influence of parameter perturbations. The amplitude of p-AKT and its variance decreases with increasing ω. For very high ω ($\log_{10}(\omega) > 0.5$), the amplitude is negligible and does not depend upon the parameters. The inset plot in Figure 6B shows the histogram of output amplitude distribution for the same MC samples. It is seen that most of the samples have low amplitudes indicating attenuation of oscillations under various combinations of the parameters. Thus, the PI3K/AKT shows three major responses to input oscillations, namely attenuation of the amplitude at all frequencies, filtering of the oscillations in frequency range, $-1 < \log_{10}(\omega) < 0.5$ and complete cutoff of oscillations in the range, $\log_{10}(\omega) > 0.5$. Earlier theoretical studies have offered an explanation for cutoff of high frequency oscillations (Gomez-Uribe et al., 2007; Wang et al., 2010) at high frequencies, short transient stimulus is not long enough as compared to the response time of the pathway, leading to filtering of the oscillations, which is then followed by complete cutoff of the signal.

In order to further quantify the influence of parameters on modulation of output amplitude, a GSA was performed for the set of MC samples with $\omega = 0.01\ \text{min}^{-1}$ and a of 0.9 (region highlighted by the rectangle in Figure 6B). A second order RS-HDMR with amplitude of p-AKT as the output function showed that first and second order indices explain 75% of the variance in the data. Figure 6C shows the first order Sobol' indices. As seen from the figure, there are three major categories of sensitive parameters that can change the output amplitude. These include, (1) parameters (including PTEN) modulating the rate of PI3K and PIP_3 activation and deactivation, (2) negative feedback parameters and (3) the activation and deactivation of insulin receptor. Parameters associated with internalization or recycling of the receptors and those associated with $PI(3,4)P_2$ do not affect the signal transfer efficiency. Figure 6D shows the second order indices for the same output. Many of the parameters with highly sensitive first order indices show important second order interactions. Importantly, parameters associated with activation and deactivation of IRS1 (Y) (k_7 and k_{-7}) show important second order contributions to these parameters, although they do not show first order contributions. In summary, the output amplitude is mainly decided by the cascade reactions directly leading up to p- AKT, the negative feedback parameters and receptor activation processes. Similar conclusions can be drawn for the other output molecules (data not shown). In this section, we had exclusively focused on transduction of noise-free input signals. However, in reality biological systems are exposed to noisy signals and it is

desirable to transduce only the main component of the signal while eliminating noise. Hence in the following sections we analyzed the efficiency of signal transduction through the PI3K pathway in the presence of noise.

3.4.2 Robust signal transfer with noise

3.4.2.1 Nominal case: To check whether a signal is transmitted robustly in the presence of noise, we subjected the system to input oscillations same as Section 3.4.1.2, but with added random noise. This is modeled as $Ins(t) = Ins(0)(1+ a \sin(\omega (t - 300))+ N(0,1))$. Here a normal random number with mean zero and variance 1 is added to the actual signal. Under this input signal, we explored the transduction of input signal to four output molecules. Figure 7 shows the same simulation as Figure 5, under identical conditions but with added noise. Figures 7B–C show that the major molecules of the pathway propagate the signal (Figure 7A) with high fidelity even in the presence of noise. For active receptor levels, noise affects the main output signal mainly during the maximum and minimum peaks, but the total deviation from the main signal is very low. This is mainly because the levels of active receptors are high at these insulin concentrations. For post-receptor molecules, the effect of noise is very negligible during the upper half of the insulin cycle when the levels of the molecules are high and these molecules are closer to their saturation levels. There is a slight influence of noise during the downward part of the cycle. This effect is more pronounce for molecules like p-AKT and p-IRS1 (Y) that are at very low levels under nominal conditions. Hence, the effect of noise will depend on the concentrations of the molecules, the effect being negligible at high concentrations and substantial at low concentrations.

3.4.2.2 Parametric dependence: In Section 3.4.1, we demonstrated that signal transduction efficiency is primarily governed by the frequency of the input signal. In addition, the internal pathway parameters had a dominant effect when the input frequency was low. In order to further study the effect of pathway parameters on the transduction of noisy signals, we subjected the pathway to low frequency oscillations (0.01 min^{-1}) at amplitude of 0.9 and evaluated the effect of varying sensitive parameters. Figure 8 shows the influence on p-AKT output for different parameter perturbations. Based on GSA of Figure 6, three main parameters were chosen, namely PTEN, K_d for negative feedback and k_1 for receptor activation. Figure 8A shows the effect of PTEN on the amplitude of p-AKT oscillations. PTEN is maintained at three levels, namely 0.5, 1.0 and 1.5. Increasing levels of PTEN increased the amplitude of the oscillations without much effect on the influence of noise. This effect is mainly due to the divergent effects of PTEN changes on molecules upstream and downstream of PIP_3. For example, increasing PTEN decreases the levels of downstream molecules like p-AKT and p-PKC-ζ (and hence p-IRS1 (S)) but it increases the levels of upstream molecules like p-IRS1 (Y). As a result, even though p-AKT decreases, there are comparatively more p-IRS1 (Y) molecules available for further activation if insulin is increased. This leads to increased amplitude of the oscillations in p-AKT with increasing PTEN, even though actual levels of p-AKT are low. The negative correlation between p-AKT and p-IRS1 (Y) under changes in PTEN was recently validated by us experimentally for the hESC system (Mathew et al., 2014).

Figure 8B shows the effect of increasing K_d, the half maximal rate of negative feedback. K_d was kept at three levels 1.2, 12 and 120. The amplitude of the oscillations decreased with increasing levels of negative feedback molecules. Increasing K_d reduces the maximal levels of negative feedback molecule PKC-ζ and hence p-IRS1 (S). This demonstrates the amplitude attenuation property of negative feedback. This effect is opposite of PTEN increase since, increasing negative feedback strength will lead to reduction in p-IRS1 (Y). Thus, the level of IRS1 (Y) affects the amplification or attenuation of the signals.

Figure 8C shows the effect of modulating the strength of receptor activation (k_1) by insulin. k_1 was varied as 6×10^6, 6×10^7 and 6×10^8. It is seen that increasing k_1 reduces the amplitude of the oscillations. For a given set of parameters, increasing k_1 leads to increased activation of the pathway and the system gets closer to the saturation regime. This is clear from the significant suppression of the upper cycle of the oscillations than the lower cycle. Although PTEN and K_d had no significant effect on the noise in the output signal of p-AKT, notable effect is seen while modulating k_1. The effect is more pronounced at high levels of k_1 and lower half of the cycle. Thus, transmission of oscillation is better at lower active receptor levels. This is mainly because decreasing k_1 leads to reduction in the response time and hence, the pathway is better able to filter fast acting changes as they are not transmitted at the beginning of the pathway.

The parameter combinations presented in this section detail the various ways of amplifying or attenuating the amplitude of signals transduced from the input insulin to downstream molecules. Parameters that lead to increase in the levels of active molecules upstream of p-AKT amplify the signal while parameters that lead to increase in negative feedback lead to attenuation of the signal. The effect of noise will primarily depend upon the concentrations of insulin and the rate of receptor activation.

4. CONCLUSIONS

In this work, we analyzed the critical signal transduction properties of an important self-renewal signaling pathway, insulin/IGF1 mediated PI3K/AKT pathway in hESCs. The focus of the work was on identifying robustness promoting mechanisms from the complex interactions of the PI3K/AKT pathway. We concentrated on two major areas: (1) maintenance of robust response in the presence of internal variability and (2) robust transfer of signals from variable and noisy input stimulus. We relied on specific quantitative robustness measures propounded by Kitano and analyzed the influence of rate parameter uncertainty and input insulin oscillations using a global sensitivity approach.

Using PTP as a control point to modulate the dynamics, we found that presence of negative feedback acts as a robustness promoting mechanism. For hESC specific parameter ranges that promote overshoot behavior in self-renewal molecule p-AKT, the system is insensitive to perturbations associated with the cascade reactions that propagate signals from the active receptors to the downstream kinases. We predict that if the system looses it negative feedback character or shifts to a regime where PTP levels are very low, it will become vulnerable to the otherwise insensitive perturbations. In such a regime, the levels of self-

renewal molecules like p-AKT will be high but also highly variable. This sets up a classical robustness tradeoff often seen in complex systems.

In the second theme, we evaluated the efficiency of signal transfer for variation in the input signal. Our results indicate that oscillations of small frequency and high amplitude are transduced down the pathway, but with amplitude attenuation. This is consistent with recent models in other cell systems, where p-AKT has been demonstrated to operate at 5 to 22 % of its dynamic range under nominal conditions (Tan et al., 2012). Our results also demonstrate that the downstream molecules follow the main signal with very high fidelity even in the presence of noise. Any modulation of upstream positive regulator IRS1 (p-IRS1 (Y)) can result in amplification or attenuation of the signals. Increasing the oscillations, however, results in a regime where significant attenuation of the amplitude may be achieved. Finally, at very high frequencies, all oscillations are cutoff. Since this region is not affected by parameter perturbations, it is clear that the PI3K/AKT pathway has an intrinsic minimal response time and when the oscillations are faster than this response time, they are not transmitted.

Application of quantitative measures of robustness can be used to finely tune the signaling pathway in hESCs to ensure that the level as well as the variability is kept within sufficient limits. Further, understanding the parameter dependences of the filtering and cut-off processes can help in the design of optimal input stimulation scenarios to modulate the pathway. Our work presents a framework towards the design of targeted growth media to maintain robust cellular fate of hESCs.

Supplementary Material

Refer to Web version on PubMed Central for supplementary material.

ACKNOWLEDGMENTS

This work was supported by NIH New Innovator Award [1DP2OD006491-01 to I.B.].

REFERENCES

Agarwal S, Holton KL, Lanza R. Efficient differentiation of functional hepatocytes from human embryonic stem cells. Stem Cells. 2008; 26:1117–1127. [PubMed: 18292207]

Alderson DL, Doyle JC. Contrasting views of complexity and their implications for network-centric infrastructures. Systems, Man and Cybernetics, Part A: Systems and Humans, IEEE Transactions on. 2010; 40:839–852.

Alva JA, Lee GE, Escobar EE, Pyle AD. Phosphatase and Tensin Homolog Regulates the Pluripotent State and Lineage Fate Choice in Human Embryonic Stem Cells. Stem Cells. 2011; 29:1952–1962. [PubMed: 21948699]

Andersen JN, Jansen PG, Echwald SM, Mortensen OH, Fukada T, Del Vecchio R, Tonks NK, Moller NP. A genomic perspective on protein tyrosine phosphatases: gene structure, pseudogenes, and genetic disease linkage. FASEB J. 2004; 18:8–30. [PubMed: 14718383]

Behar M, Barken D, Werner SL, Hoffmann A. The Dynamics of Signaling as a Pharmacological Target. Cell. 2013; 155:448–461. [PubMed: 24120141]

Behar M, Hoffmann A. Understanding the temporal codes of intra-cellular signals. Curr Opin Genet Dev. 2010; 20:684–693. [PubMed: 20956081]

Bendall SC, Stewart MH, Menendez P, George D, Vijayaragavan K, Werbowetski-Ogilvie T, Ramos-Mejia V, Rouleau A, Yang J, Bossé M. IGF and FGF cooperatively establish the regulatory stem cell niche of pluripotent human cells in vitro. Nature. 2007; 448:1015–1021. [PubMed: 17625568]

Blüthgen N, Herzel H. How robust are switches in intracellular signaling cascades? Journal of theoretical biology. 2003; 225:293–300. [PubMed: 14604583]

Bluthgen N, Legewie S. Robustness of signal transduction pathways. Cell Mol Life Sci. 2013; 70:2259–2269. [PubMed: 23007845]

Cahan P, Daley GQ. Origins and implications of pluripotent stem cell variability and heterogeneity. Nat Rev Mol Cell Biol. 2013; 14:357–368. [PubMed: 23673969]

Chen, L.; Wang, R.; Li, C.; Aihara, K. Modeling Biomolecular Networks in Cells. Springer; 2010.

Csete ME, Doyle JC. Reverse engineering of biological complexity. Science. 2002; 295:1664–1669. [PubMed: 11872830]

D'Amour KA, Bang AG, Eliazer S, Kelly OG, Agulnick AD, Smart NG, Moorman MA, Kroon E, Carpenter MK, Baetge EE. Production of pancreatic hormone-expressing endocrine cells from human embryonic stem cells. Nat Biotechnol. 2006; 24:1392–1401. [PubMed: 17053790]

Dalton S. Signaling networks in human pluripotent stem cells. Curr Opin Cell Biol. 2013; 25:241–246. [PubMed: 23092754]

Desbordes SC, Placantonakis DG, Ciro A, Socci ND, Lee G, Djaballah H, Studer L. High-throughput screening assay for the identification of compounds regulating self-renewal and differentiation in human embryonic stem cells. Cell stem cell. 2008; 2:602–612. [PubMed: 18522853]

Eissing T, Allgower F, Bullinger E. Robustness properties of apoptosis models with respect to parameter variations and intrinsic noise. Syst Biol (Stevenage). 2005; 152:221–228. [PubMed: 16986264]

Feil, B.; Kucherenko, S.; Shah, N. Comparison of monte carlo and quasi monte carlo sampling methods in high dimensional model representation. IEEE Advances in System Simulation, 2009; First International Conference on SIMUL '09; 2009. p. 12-17.

Fisher J, Henzinger TA. Executable cell biology. Nat Biotechnol. 2007; 25:1239–1249. [PubMed: 17989686]

Fujita KA, Toyoshima Y, Uda S, Ozaki Y, Kubota H, Kuroda S. Decoupling of receptor and downstream signals in the Akt pathway by its low-pass filter characteristics. Sci Signal. 2010; 3:ra56. [PubMed: 20664065]

Gafni O, Weinberger L, Mansour AA, Manor YS, Chomsky E, Ben-Yosef D, Kalma Y, Viukov S, Maza I, Zviran A, Rais Y, Shipony Z, Mukamel Z, Krupalnik V, Zerbib M, Geula S, Caspi I, Schneir D, Shwartz T, Gilad S, Amann-Zalcenstein D, Benjamin S, Amit I, Tanay A, Massarwa R, Novershtern N, Hanna JH. Derivation of novel human ground state naive pluripotent stem cells. Nature. 2013; 504:282–286. [PubMed: 24172903]

Giri L, Mutalik VK, Venkatesh KV. A steady state analysis indicates that negative feedback regulation of PTP1B by Akt elicits bistability in insulin-stimulated GLUT4 translocation. Theoretical Biology and Medical Modelling. 2004; 1:2. [PubMed: 15291972]

Gomez-Uribe C, Verghese GC, Mirny LA. Operating regimes of signaling cycles: statics, dynamics, and noise filtering. Plos Computational Biology. 2007; 3:e246. [PubMed: 18159939]

Hindmarsh, AC. ODEPACK, A Systematized Collection of ODE Solvers. In: Stepleman, RS., et al., editors. IMACS transactions on scientific computation. Vol. 1. North-Holland, Amsterdam: 1983. p. 55-64.1, 55–64.

Kiel C, Yus E, Serrano L. Engineering signal transduction pathways. Cell. 2010; 140:33–47. [PubMed: 20085704]

Kiselyov VV, Versteyhe S, Gauguin L, De Meyts P. Harmonic oscillator model of the insulin and IGF1 receptors' allosteric binding and activation. Mol Syst Biol. 2009; 5:243. [PubMed: 19225456]

Kitano H. Biological robustness. Nat Rev Genet. 2004; 5:826–837. [PubMed: 15520792]

Kitano H. Towards a theory of biological robustness. Mol Syst Biol. 2007; 3:137. [PubMed: 17882156]

Kitano H. Violations of robustness trade-offs. Mol Syst Biol. 2010; 6:384. [PubMed: 20571533]

Kleinman, HK.; Martin, GR. Matrigel: basement membrane matrix with biological activity. Vol. 15. Elsevier; 2005. p. 378-386.

Kubota H, Noguchi R, Toyoshima Y, Ozaki Y-i, Uda S, Watanabe K, Ogawa W, Kuroda S. Temporal coding of insulin action through multiplexing of the AKT pathway. Molecular cell. 2012; 46:820–832. [PubMed: 22633957]

Kwei, EC.; Sanft, KR.; Petzold, LR.; Doyle, FJ, III. Systems analysis of the insulin signaling pathway; In Proceedings of the 17th IFAC World Congress; Coex, South Korea. 2008.

Li G, Rabitz H, Yelvington PE, Oluwole OO, Bacon F, Kolb CE, Schoendorf J. Global sensitivity analysis for systems with independent and/or correlated inputs. The Journal of Physical Chemistry A. 2010; 114:6022–6032. [PubMed: 20420436]

Li GY, Rabitz H. General formulation of HDMR component functions with independent and correlated variables. Journal of Mathematical Chemistry. 2012; 50:99–130.

Li W, Li K, Wei W, Ding S. Chemical approaches to stem cell biology and therapeutics. Cell stem cell. 2013; 13:270–283. [PubMed: 24012368]

Ludwig T, Thomson JA. Defined, feeder-independent medium for human embryonic stem cell culture. Curr Protoc Stem Cell Biol. 2007; Chapter 1(Unit 1C 2)

Luni C, Doyle FJ III. Robust multi drug therapy design and application to insulin resistance in type 2 diabetes. International Journal of Robust and Nonlinear Control. 2011; 21:1730–1741.

Luni C, Sanft KR, Petzold LR, Doyle FJ III. Modelling of Detailed Insulin Receptor Kinetics Affects Sensitivity and Noise in the Downstream Signalling Pathway.

Ma L, Iglesias PA. Quantifying robustness of biochemical network models. BMC bioinformatics. 2002; 3:38. [PubMed: 12482327]

Mahadev K, Wu XD, Zilbering A, Zhu L, Lawrence JTR, Goldstein BJ. Hydrogen peroxide generated during cellular insulin stimulation is integral to activation of the distal insulin signaling cascade in 3T3-L1 adipocytes. Journal of Biological Chemistry. 2001; 276:48662–48669. [PubMed: 11598110]

Masel J, Siegal ML. Robustness: mechanisms and consequences. Trends Genet. 2009; 25:395–403. [PubMed: 19717203]

Mathew S, Jaramillo M, Zhang X, Zhang LA, Soto-Gutiérrez A, Banerjee I. Analysis of alternative signaling pathways of endoderm induction of human embryonic stem cells identifies context specific differences. BMC systems biology. 2012; 6:154. [PubMed: 23241383]

Mathew S, Sankaramanivel S, Mamiya H, Banerjee I. Regulatory interactions maintaining self-renewal of human embryonic stem cells as revealed through systems analysis of PI3K/AKT pathway. Bioinformatics. 2014 Accepted, under preparation.

Murry CE, Keller G. Differentiation of embryonic stem cells to clinically relevant populations: lessons from embryonic development. Cell. 2008; 132:661–680. [PubMed: 18295582]

Nelson TJ, Behfar A, Yamada S, Martinez-Fernandez A, Terzic A. Stem cell platforms for regenerative medicine. Clin Transl Sci. 2009; 2:222–227. [PubMed: 19779576]

Nguyen LK, Matallanas D, Croucher DR, von Kriegsheim A, Kholodenko BN. Signalling by protein phosphatases and drug development: a systems-centred view. FEBS J. 2013; 280:751–765. [PubMed: 22340367]

Ogunnaike, BA.; Ray, WH. Process dynamics, modeling, and control. Vol. 9. New York: Oxford University Press; 1994.

Rizk A, Batt G, Fages F, Soliman S. A general computational method for robustness analysis with applications to synthetic gene networks. Bioinformatics. 2009; 25:i169–i178. [PubMed: 19477984]

Scott LM, Lawrence HR, Sebti SM, Lawrence NJ, Wu J. Targeting protein tyrosine phosphatases for anticancer drug discovery. Current pharmaceutical design. 2010; 16:1843. [PubMed: 20337577]

Seborg, DE.; Mellichamp, DA.; Edgar, TF.; Doyle, FJ, III. Process dynamics and control. John Wiley & Sons; 2010.

Sedaghat AR, Sherman A, Quon MJ. A mathematical model of metabolic insulin signaling pathways. Am J Physiol Endocrinol Metab. 2002; 283:E1084–E1101. [PubMed: 12376338]

Singh AM, Reynolds D, Cliff T, Ohtsuka S, Mattheyses AL, Sun YH, Menendez L, Kulik M, Dalton S. Signaling Network Crosstalk in Human Pluripotent Cells: A Smad2/3-Regulated Switch that Controls the Balance between Self-Renewal and Differentiation. Cell stem cell. 2012; 10:312–326. [PubMed: 22385658]

Smith GR, Shanley DP. Computational modelling of the regulation of Insulin signalling by oxidative stress. BMC Syst Biol. 2013; 7:41. [PubMed: 23705851]

Sobol′ IM. Global sensitivity indices for nonlinear mathematical models and their Monte Carlo estimates. Mathematics and computers in simulation. 2001; 55:271–280.

Stelling J, Sauer U, Szallasi Z, Doyle FJ 3rd, Doyle J. Robustness of cellular functions. Cell. 2004; 118:675–685. [PubMed: 15369668]

Tan SX, Ng Y, Meoli CC, Kumar A, Khoo PS, Fazakerley DJ, Junutula JR, Vali S, James DE, Stockli J. Amplification and demultiplexing in insulin-regulated Akt protein kinase pathway in adipocytes. Journal of Biological Chemistry. 2012; 287:6128–6138. [PubMed: 22207758]

Thomson JA, Itskovitz-Eldor J, Shapiro SS, Waknitz MA, Swiergiel JJ, Marshall VS, Jones JM. Embryonic stem cell lines derived from human blastocysts. Science. 1998; 282:1145–1147. [PubMed: 9804556]

Tian T, Wu F. Robustness Analysis of the PI3K/AKT Cell Signaling Module. Journal of Medical and Bioengineering. 2013; 2:93–97.

Toyoshima Y, Kakuda H, Fujita KA, Uda S, Kuroda S. Sensitivity control through attenuation of signal transfer efficiency by negative regulation of cellular signalling. Nature communications. 2012; 3:743.

Wang L, Xin J, Nie Q. A critical quantity for noise attenuation in feedback systems. Plos Computational Biology. 2010; 6:e1000764. [PubMed: 20442870]

Whitacre JM. Biological robustness: paradigms, mechanisms, and systems principles. Front Genet. 2012; 3:67. [PubMed: 22593762]

Winterbach W, Van Mieghem P, Reinders M, Wang H, de Ridder D. Topology of molecular interaction networks. BMC Syst Biol. 2013; 7:90. [PubMed: 24041013]

Yao S, Chen S, Clark J, Hao E, Beattie GM, Hayek A, Ding S. Long-term self-renewal and directed differentiation of human embryonic stem cells in chemically defined conditions. Proc Natl Acad Sci U S A. 2006; 103:6907–6912. [PubMed: 16632596]

Yoon BS, Jun EK, Park G, Jun Yoo S, Moon JH, Soon Baik C, Kim A, Kim H, Kim JH, Young Koh G. Optimal Suppression of Protein Phosphatase 2A Activity Is Critical for Maintenance of Human Embryonic Stem Cell Self_Renewal. Stem Cells. 2010; 28:874–884. [PubMed: 20306465]

Zamora-Sillero E, Hafner M, Ibig A, Stelling J, Wagner A. Efficient characterization of high-dimensional parameter spaces for systems biology. BMC Syst Biol. 2011; 5:142. [PubMed: 21920040]

Zhang ZY. Functional studies of protein tyrosine phosphatases with chemical approaches. Biochim Biophys Acta. 2005; 1754:100–107. [PubMed: 16226063]

HIGHLIGHTS

1. Quantitative features of robustness of PI3K/AKT pathway were investigated.
2. Robust dynamic response is ensured by negative feedback under nominal AKT behavior.
3. Signal transfer from input to AKT shows noise filtering and amplitude attenuation.
4. Processes upstream and downstream of PIP_3 show divergent effects on signal transfer.

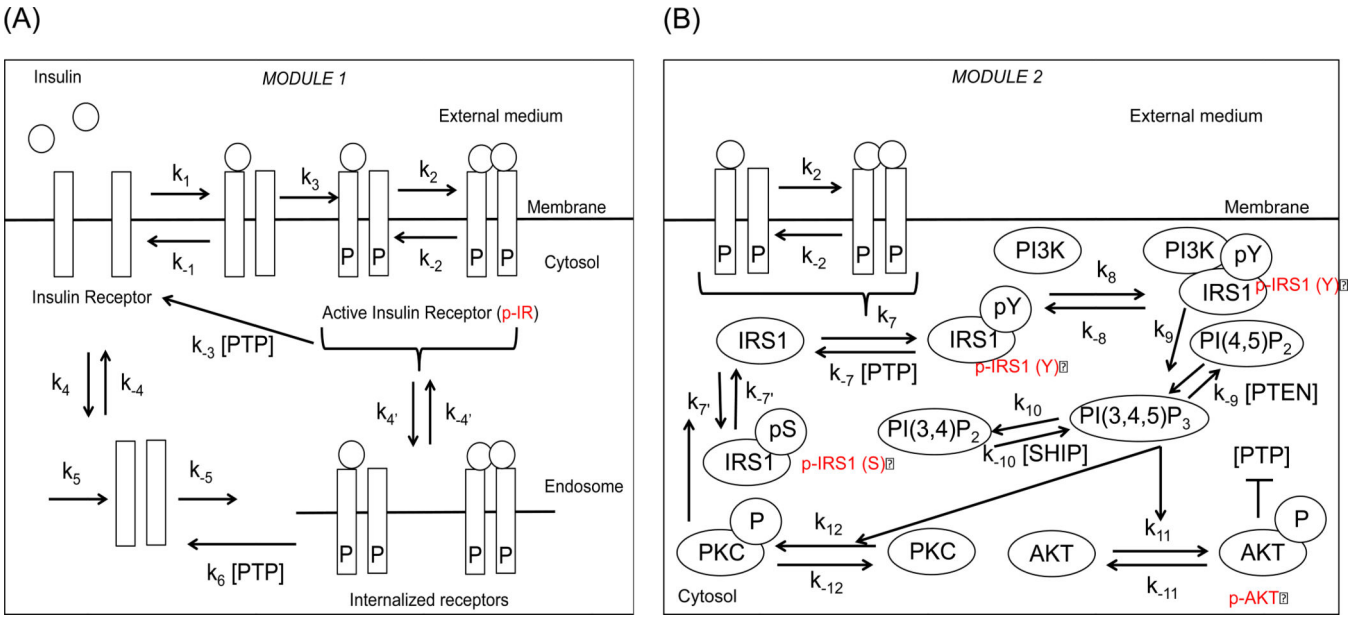

Figure 1. Signal transduction in PI3K/AKT pathway

(A) Module 1: Receptor level processes including receptor activation, internalization and recycling. **(B)** Module 2: Post receptor signaling processes resulting in the activation of AKT. Notice the negative feedback due to serine (S) phosphorylation of IRS1 that inhibits the tyrosine (Y) phosphorylation of IRS1. PTEN and SHIP act as negative regulators of PIP_3. PTP acts as a negative regulator of molecules belonging to both modules, namely active IR and tyrosine phosphorylated IRS1. Active AKT inhibits PTP and sets up a double negative feedback loop.

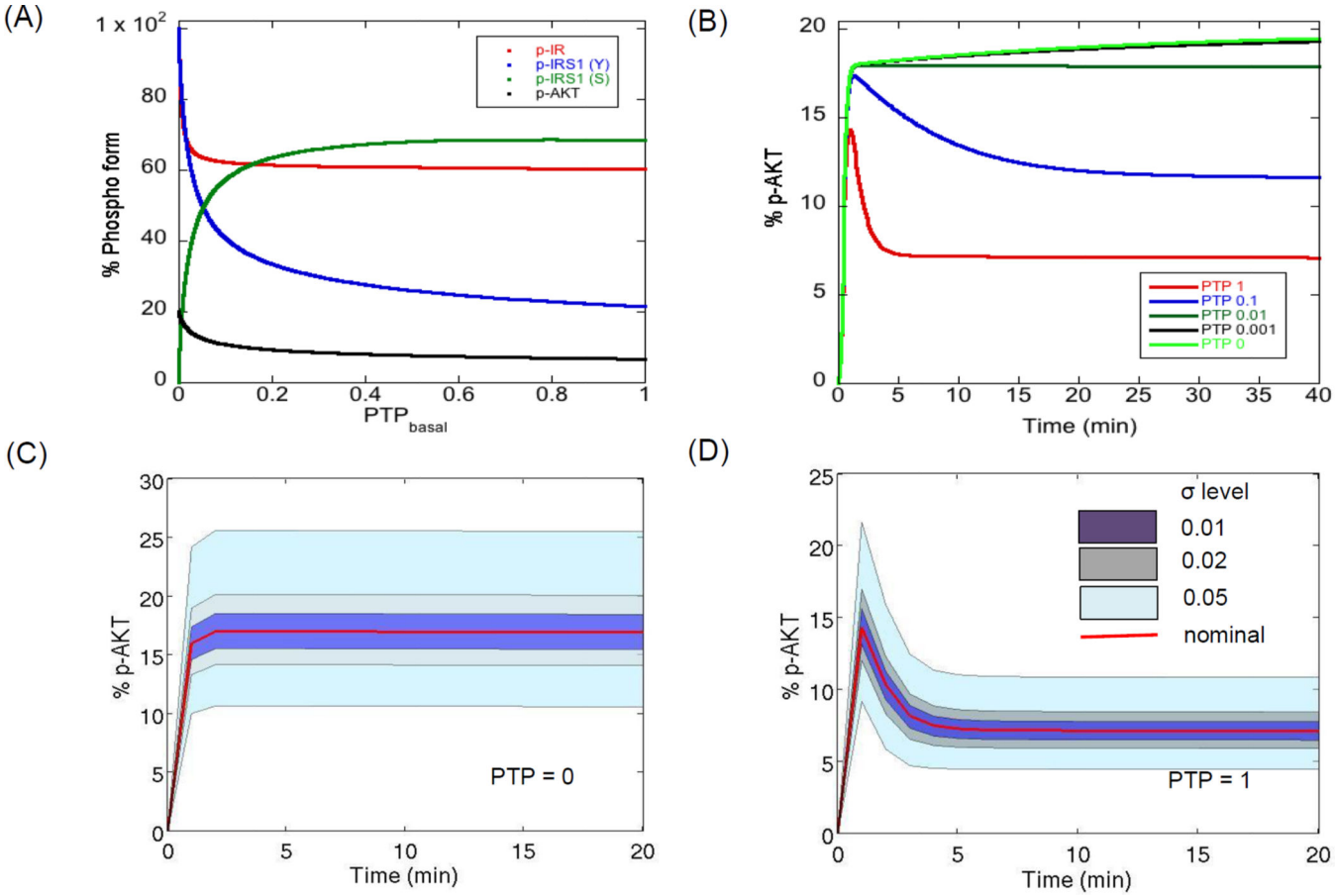

Figure 2. Negative modulation of PI3K/AKT pathway molecules by PTP

(A) Influence of basal PTP levels on steady state levels of the major outputs. The kinetic parameters of the model are kept at their nominal levels and only the levels of PTP are varied. It is observed that the steady state levels of the molecules are highly sensitive to PTP when basal PTP level is less than 1% of the nominal level. **(B)** Dynamics of p-AKT under different basal PTP levels. Under nominal conditions, we see the typical overshoot behavior, contributed by negative feedback, while very low PTP levels result in a first order behavior. Insulin levels are kept constant at 10^{-7} M. **(C–D)** Influence of variations in kinetic parameters on the dynamics of p-AKT when PTP = 0 and PTP = 1. Each free parameter is varied according to the relation in Equation (1) assuming a uniform distribution around the nominal for two extreme PTP levels. Plotted here is the cluster of profiles (shown by banded regions) for different degrees of parameter perturbations. The red curve shows the nominal profile. The insulin concentration is kept constant at saturation (10^{-7} M).

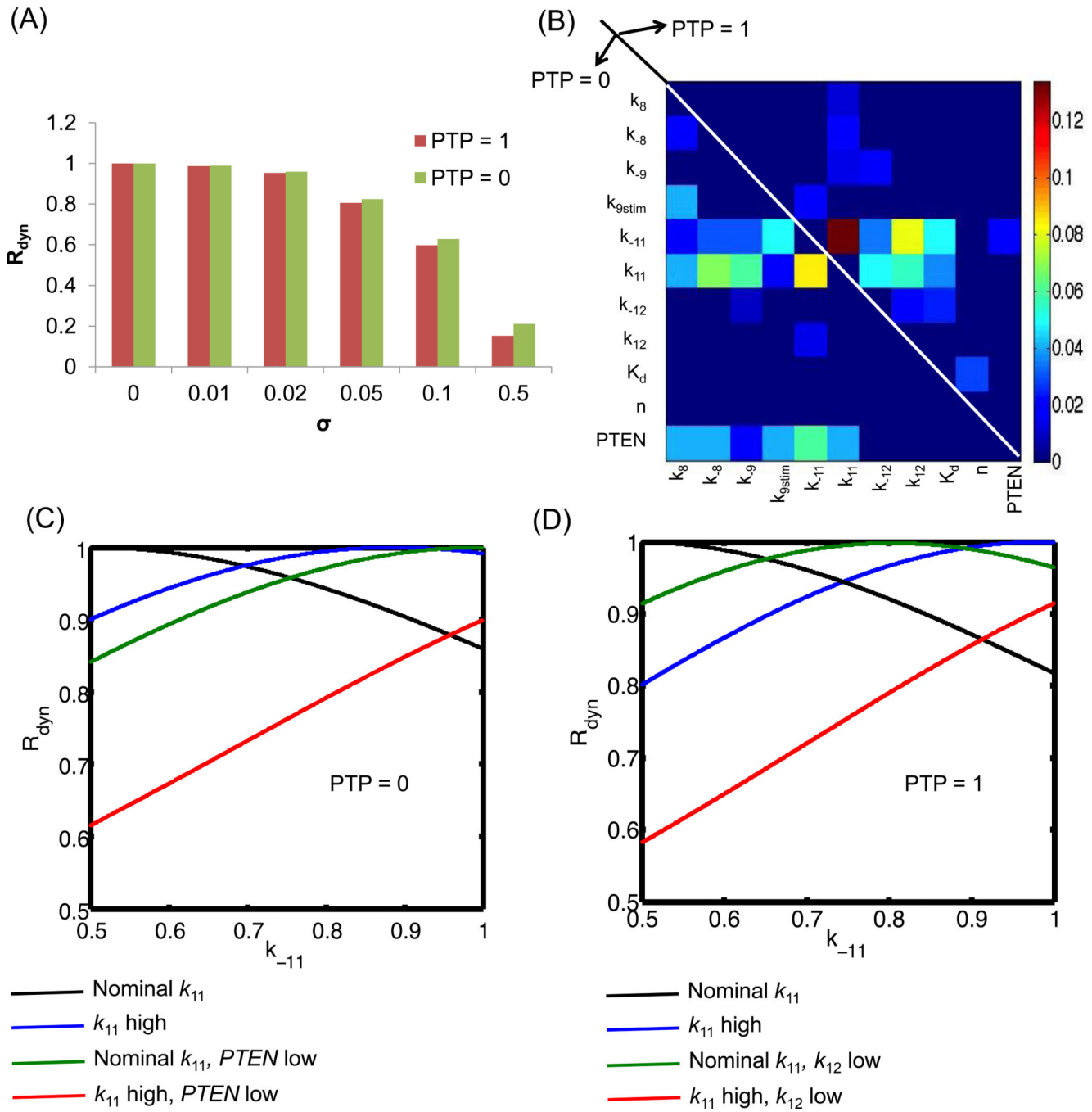

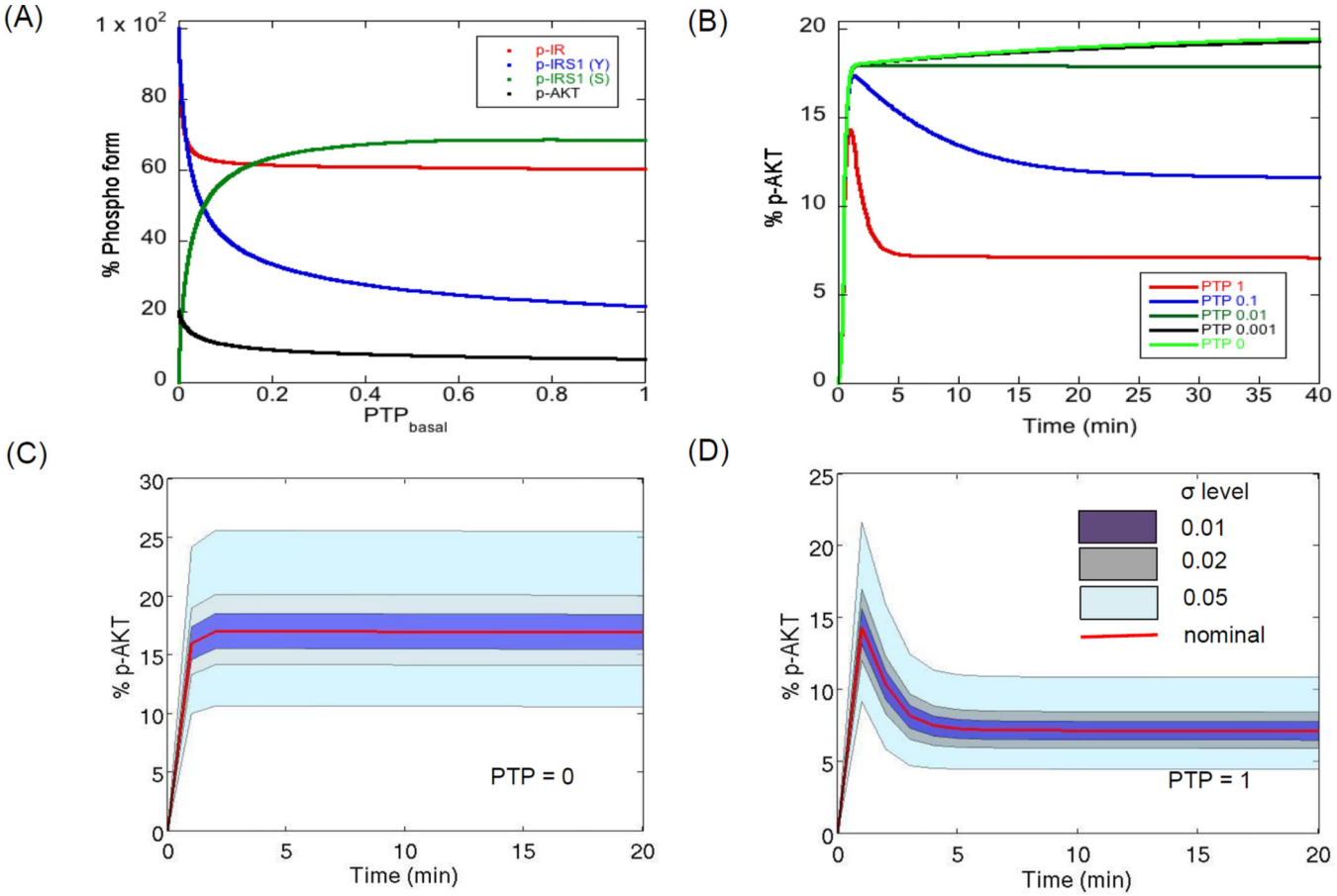

Figure 3. Relative contributions of kinetic processes to robust p-AKT dynamics

(A) Overall robustness of p-AKT dynamics to parameter perturbations for extreme PTP levels. Robustness is measured as deviation of p-AKT dynamics from expected dynamics (Figure 2C–D) under PTP = 0 and PTP = 1. This plot presents the average robustness score given by Equation (3) for different levels of σ. **(B)** Contributions of the parameters to the robustness score. The heatmap presents the second order Sobol' indices contributing to variations in individual robustness score in the perturbed parameter space for a given σ of 0.05. The second order indices were the most prominent and contributed to 70% of the variance. The common contributors are k_{11} and k_{-11}. Among the secondary contributors, most of the reactions directly influencing PI3K, PIP_3 levels are prominent under PTP = 0 and reactions associated with PKC-ζ and negative feedback are prominent under PTP = 1. Thus, the model is robust to PI3K and PIP_3 perturbations when PTP = 1 and is not robust to these perturbations when PTP = 0. **(C–D)** Modulation of robustness by perturbation of multiple sensitive processes, **(C)** Results for PTP = 0. Black curve shows the influence of the de-phosphorylation rate (k_{-11}) on the robustness measure. Simultaneous increase in the phosphorylation rate (k_{11}, blue) or reduction in PTEN levels (green) can rescue the negative effects of increase in k_{-11}. However, all three perturbations together is detrimental. Note that all the non-perturbed parameters are kept at their nominal levels. (D) Results for PTP = 1. Here the effect of increase in the phosphorylation rate (k_{11}) and decrease in the negative feedback parameter (k_{12}) are studied. We see similar observations as (C). For both the plots

in C and D, the X-axis represents the normalized value of the parameter k_{-11} converted to the range [0.5, 1]. High and low values of the other parameters indicate the end points of the parameter ranges for sigma 0.05. Opposite conclusions hold when the parameter k_{-11} is varied in the range [0, 0.5]. For example, for PTP = 0, the value of k_{11} should be decreased and PTEN increased when k_{-11} is in the range [0,0.5] to increase evaluation function.

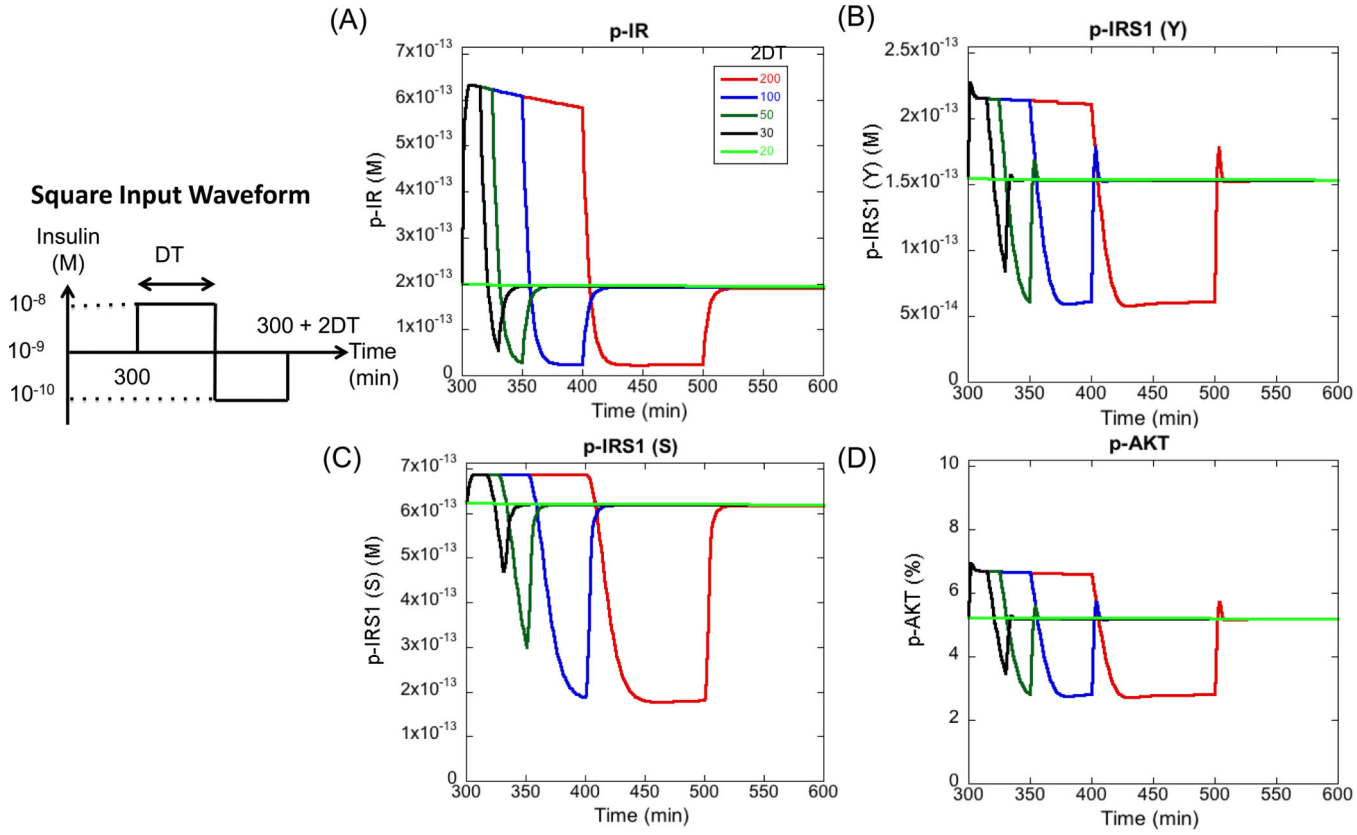

Figure 4. Response of pathway outputs to different cycle periods in insulin stimulus

Four outputs are plotted here. **(A)** Surface p-IR **(B)** p-IRS1 (Y) **(C)** p-IRS1 (S) and **(D)** p-AKT. Insulin levels are subjected to a cycle, modeled as a single square waveform. The duration of the waveform is varied and the resulting cycle in the output is measured. DT stands for duration of half of the cycle. For most cycle durations, the cycle is faithfully transmitted down the pathway, but for a duration of less than 20 minutes, the cycle is no longer transmitted. This is seen as a flat curve where the level of the output remains stable at the pre-cycle steady state. Therefore, any oscillations with a frequency greater than 0.05 min^{-1} (or period less than 20 minutes) will be cut-off by the pathway (for the current waveform). All the results in this section are generated by numerical integration of the ODEs.

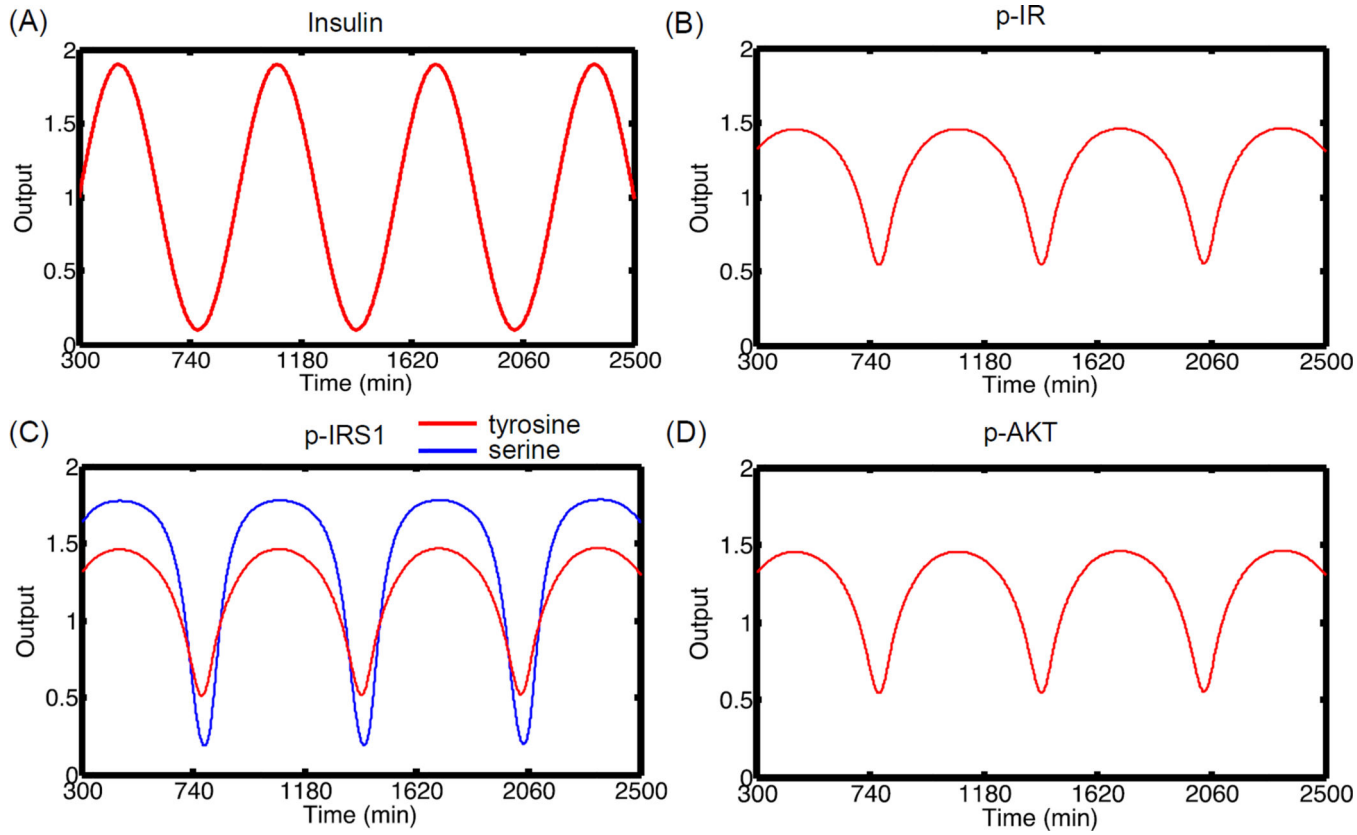

Figure 5. Signal propagation in the pathway without noise

(A) Insulin stimulus oscillations with time. The pathway is first allowed to reach steady state for insulin concentration of 10^{-9} M. At 300 min, the levels of insulin are subjected to oscillations with $\omega = 0.01$ and amplitude of 0.9. **(B)** p-IR oscillations with time. **(C)** p-IRS1 (Y) and (S) oscillations with time **(D)** p-AKT oscillations with time. In general, the signal is transmitted with attenuation down the pathway for molecules directly upstream of p-AKT. The amplitude is not damped significantly for p-IRS1 (S). For this figure, each output is normalized to the mean value of the oscillations.

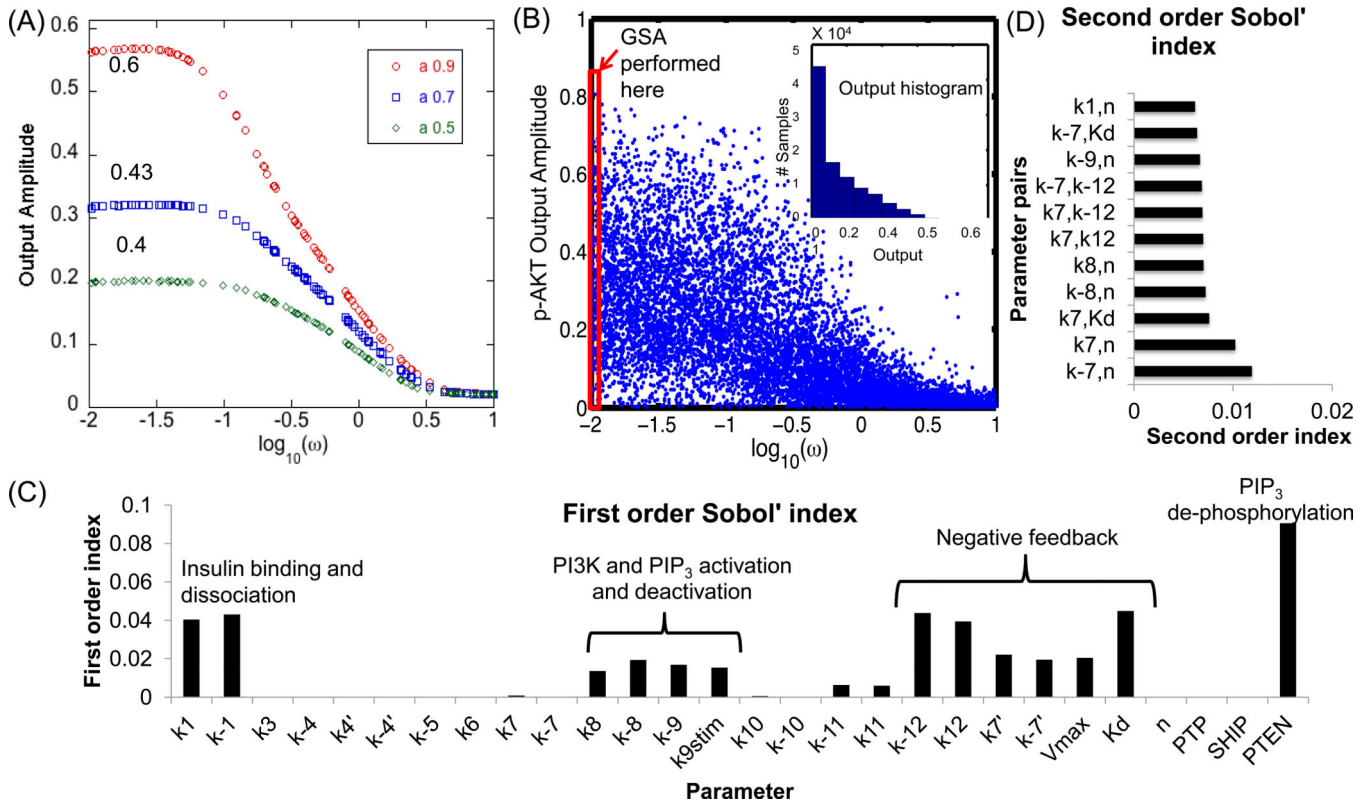

Figure 6. Parametric dependence of signal transfer efficiency to p-AKT

(A) Influence of input amplitude on output oscillations. The amplitude of the input is kept at three levels 0.9, 0.7 and 0.5 for the nominal conditions. For low frequencies, we see a flat response, with a fixed but lower amplitude in the p-AKT output. For frequency higher than 0.1, the amplitude falls down linearly to negligible values. All parameters and initial concentrations are kept at the nominal values and PTP is kept at 1. The numbers indicated in the flat region represent the ratio of output amplitude to input amplitude. **(B)** Influence of input frequency on the output amplitude of p-AKT in the entire parameter space. The input amplitude is kept constant at 0.9. The value of σ of 0.5 is selected for the analysis. PTP levels are kept at 1. In general, frequency values greater that 0.5 (log scale) show very low output amplitude. GSA is performed in the region highlighted by the rectangle. Parameter variations have the most effect at lower frequencies. Inset: Histogram of output distribution. The Y-axis denotes the number of samples out of 10^5. **(C)** First order Sobol' indices showing influence of different parameters on the output amplitude when input amplitude is kept constant at 0.9 and a frequency of 0.01 min^{-1}. The value of σ of 0.5 is selected for the analysis. **(D)** Second order Sobol' indices.

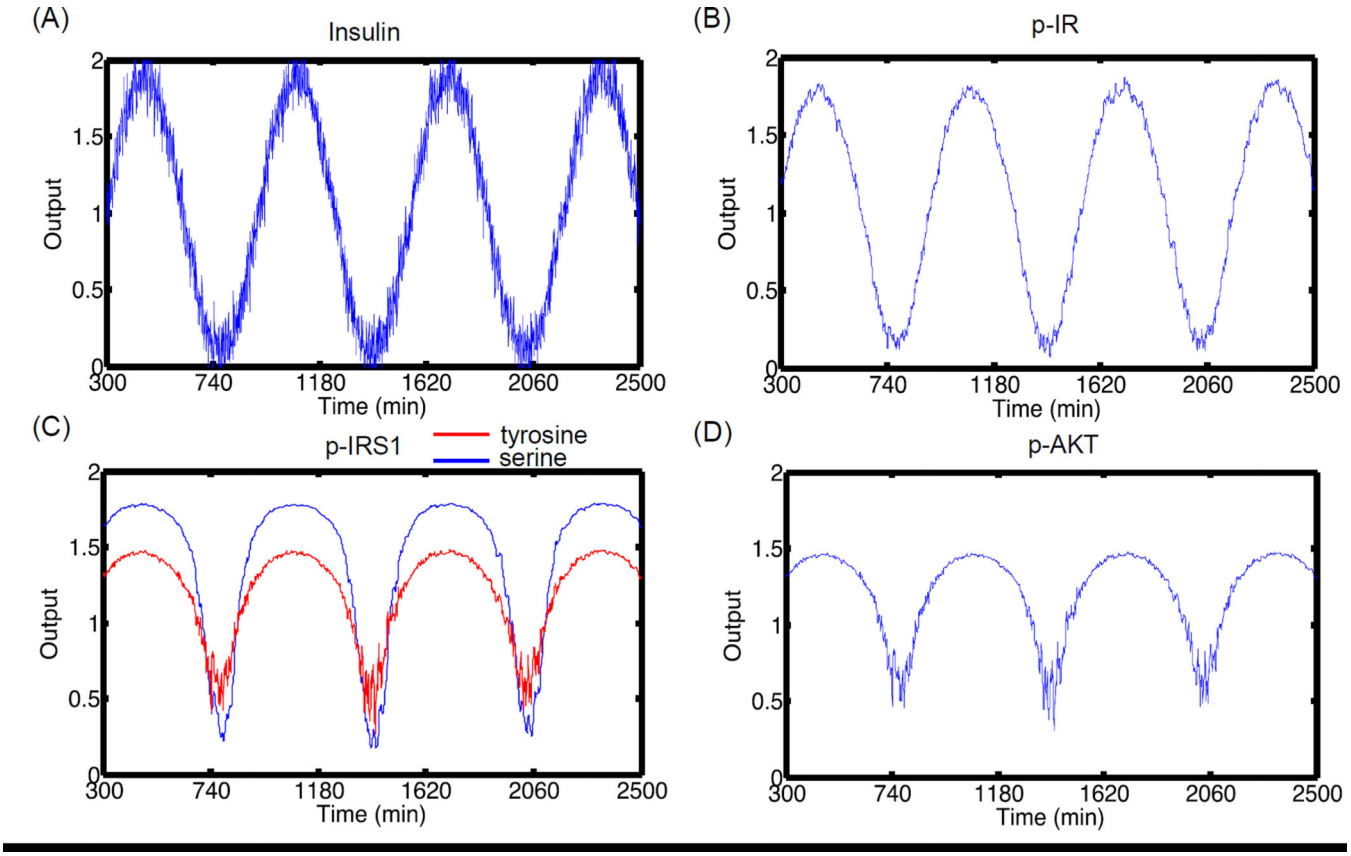

Figure 7. Signal propagation in the pathway under noisy stimulus

(A) Insulin stimulus oscillations with time. Random normal noise is added to the main signal. The pathway is first allowed to reach steady state for insulin concentration of 10^{-9} M. At 300 min, the levels of insulin are subjected to oscillations with $\omega = 0.01$ and amplitude = 0.9. **(B)** p-IR oscillations with time. **(C)** p-IRS1 (Y) and (S) oscillations with time **(D)** p-AKT oscillations with time. The output values are normalized to the mean value during the oscillations. The signal is propagated with high fidelity even in the presence of noise. The effect of noise is dominant during the down half of the cycle when the levels of molecules are low.

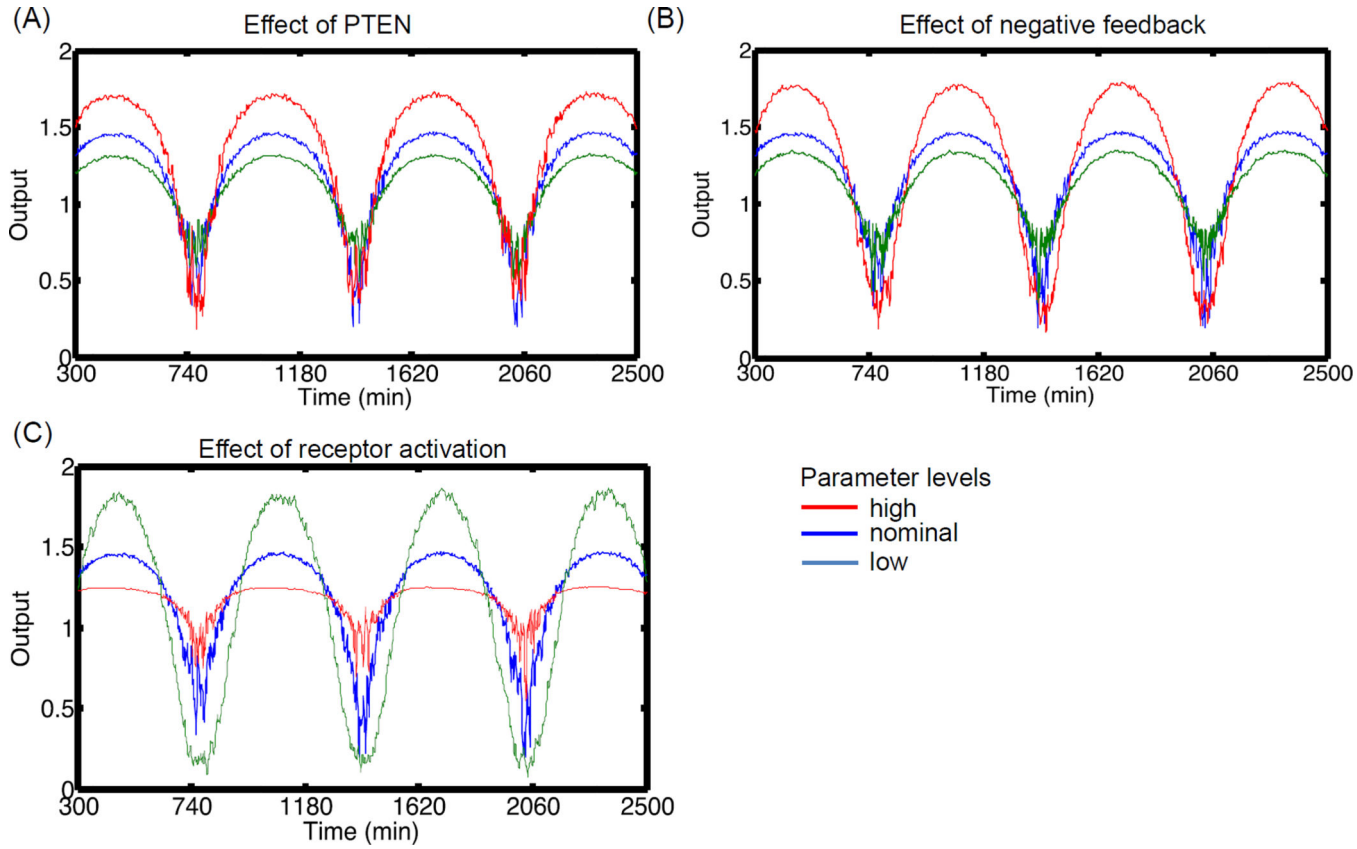

Figure 8. Effect of parameters on robust signal transfer to p-AKT in the presence of noise

For each plot, three values of the parameter are chosen based on the nominal condition. The input insulin oscillation is same as Figure 7. **(A)** Effect of PTEN. PTEN is kept at 0.5, 1.0 and 1.5. **(B)** Effect of negative feedback parameter, K_d. Increasing strength of negative feedback leads to attenuation of output amplitude. **(C)** Effect of receptor activation rates. Increasing active receptor levels can lead to suppression of the signal due to saturation of the receptors. Note that all the profiles are normalized to the mean levels during the oscillations.

Table 1

Free input parameters used for the MC simulation and their nominal values

No.	Symbol	Nominal value
M1		
1	k_1	6×10^7 $M^{-1} \cdot min^{-1}$
2	k_{-1}	0.2 min^{-1}
3	k_3	2500 min^{-1}
4	k_{-4}	0.003 min^{-1}
5	$k_{4'}$	2.1×10^{-3} min^{-1}
6	$k_{-4'}$	2.1×10^{-4} min^{-1}
7	k_{-5}	1.67×10^{-18} min^{-1}
8	k_6	0.461 min^{-1}
M2		
9	$\frac{k_7}{IR_p}$	4.64×10^{12} $M^{-1} \cdot min^{-1}$
10	k_{-7}	1.396 min^{-1}
11	k_8	7.06×10^{11} $M^{-1} \cdot min^{-1}$
12	k_{-8}	10 min^{-1}
13	k_{-9}	42.15 min^{-1}
14	k_{9stim}	4.96×10^{14} $M^{-1} \cdot min^{-1}$
15	k_{10}	2.96 min^{-1}
16	k_{-10}	2.77 min^{-1}
17	$k_{7'}$	0.347 min^{-1}
18	$k_{-7'}$	0.0858 min^{-1}
19	V_{max}	20
20	K_d	12
21	n	4
22	$[PTP]_{basal}$	1.00
23	$[SHIP]$	1.00
24	$[PTEN]$	1.00
25	k_{11}	0.693 min^{-1}
26	k_{-11}	0.0693 min^{-1}
27	k_{12}	0.693 min^{-1}
28	k_{-12}	0.0693 min^{-1}